JOURNAL OF COMPUTATIONAL PHYSICS 97, 30–52 (1991)

On the Accuracy of the Spectral Interpolation Methods for Sampled Pseudoperiodic Signals

D. R. RAJAONA AND P. SULMONT

Laboratoire d'Hydrodynamique Navale URA 1217 CNRS, ENSM Nantes, France

Received October 31, 1989; revised September 14, 1990

The accuracy of a spectral interpolation method is studied on sampled pseudoperiodic signals. An attempt is made to compute the accuracy of the characteristics of a particular component in terms of the remaining components contribution. The weighting effect is shown to improve the characteristics computation by reducing the remaining components contribution to an order of $1/N^3$, where N is the number of the samples. The noise effect and the proximity effect are analyzed and the spectral interpolation is compared with a time domain method derived from a Kumaresan Tufts procedure. © 1991 Academic Press, Inc.

I. INTRODUCTION

The analysis of a large number of physical phenomena requires calculations of periodic or pseudoperiodic components of various signals given by the measurements devices output. A set of discrete values corresponding to the time evolution of a signal must generally be analyzed. These values are usually obtained by sampling at regular time intervals of parameters describing the evolution of the phenomenon. Numerical results must often be analyzed in a similar manner as shown in [1, 2].

A line shape fitting method based on the analysis of the peaks in the discrete spectrum has been described in [3] for identifying pseudoperiodic components of a signal defined by a set of discrete values for which no weighting function is used. The purpose of this paper is to study the accuracy of such methods and to explain the expected improvement by using weighting functions. The "line shape fitting method" is in some sense an interpolation of the values defined in the frequency domain; therefore the method is called "a spectral interpolation."

II. THE SPECTRAL INTERPOLATION METHOD

II.1. *Background*

Let us consider a signal $g(t)$ sampled at regular time $t_r = rT/N$, where T is the duration of the observation in seconds, N is the number of samples. And we have $0 \leqslant r \leqslant N-1$. In other words T is the width of the window function which will be

0021-9991/91 $3.00

used for the analysis of the complete signal $g(t)$ defined in the time interval $-\infty < t < +\infty$. Furthermore we define:

$$g_r = g(t_r), \qquad r = 0, 1, ..., N-1. \tag{1}$$

These sampled data are supposed to satisfy the Shannon condition (sampling frequencies are greater than twice the largest frequency of the signal) in such a way that no aliasing phenomenon is present [4, 5].

The discrete Fourier transform of the function $g(t)$ corresponding to the frequency interval $1/T$ is given by Eq. (2):

$$G_j = \frac{1}{N} \sum_{r=0}^{N-1} g_r \exp(-i2\pi rj/N), \qquad j = 0, 1, ..., N/2. \tag{2}$$

In general, the values G_j do not provide the exact spectrum of the function $g(t)$; particularly if periodic components are present in the signal, the peaks of the spectrum are not equal to the amplitude of the periodic components except for very special cases for which the frequency peak is an integer multiple of $1/T$; this has been shown to be a result of the leakage effect [3]. Thus it is not possible to determine the amplitude and the frequency of the various components in the signal from the knowledge of the G_j values. The spectral interpolation described in [3] is useful to compute the values of amplitudes and frequencies.

II.2. *Definition of the Pseudoperiodic Signals*

The signals concerned with the method are assumed to consist of a superposition of a finite number of very distinct and weakly damped periodic components. We thus have

$$g_r = \frac{1}{2} \sum_{k=0}^{N-1} A_k \exp(i\Omega_k t_r) + \bar{A}_k \exp(-i\bar{\Omega}_k t_r) + w(t_r), \qquad r = 0, 1, ..., N-1, \tag{3a}$$

for a real signal and

$$g_r = \sum_{k=0}^{N-1} A_k \exp(i\Omega_k t_r) + w(t_r), \qquad r = 0, 1, ..., N-1, \tag{3b}$$

for a complex signal, where we have

$$A_k = a_k + ib_k \tag{4}$$

$$\Omega_k = i\lambda_k + \omega_k \tag{5}$$

with a_k, b_k, λ_k, ω_k real and $|\lambda_k| \ll 1$; $w(t_r)$ represents a low level noise.

As was shown in [3], the integer k takes values between 0 and $N-1$; however, only some values of A_k are nonzero since the signal is assumed to consist of distinct

components. For the sake of simplicity, we only present the calculation related to a complex signal. For a real signal the analysis needs to be slightly modified but the procedure for numerical calculation is essentially identical; specifically, the amplitude of a real signal as computed by using an algorithm based on the input of a complex signal only needs to be multiplied by two.

The use of weighting functions different from the rectangular window function is expected to provide more accurate values of the pseudoperiodic components; specifically by reducing the so-called leakage effect as described in Harris [6]. This paper concerns only the effect of a Hanning window although the method can be applied to other weighting functions. We thus define the weighted signal as

$$g_r^h = h_r g_r, \qquad r = 0, 1, ..., N-1, \tag{6}$$

where

$$h_r = 1 \tag{7}$$

for a rectangular window

$$h_r = 1 - \tfrac{1}{2}[\exp(i2\pi r/N) + \exp(-i2\pi r/N)] \qquad r = 0, 1, ..., N-1 \tag{8}$$

for a Hanning window.

II.3. *Error Computation*

II.3.1. *Rectangular Window*

For a rectangular window, Eqs. (2), (3b), and (6) yield

$$G_j = \frac{1}{N}\sum_{k=0}^{N-1} A_k \frac{1-\exp[-\lambda_k T + i(\omega_k T - 2\pi j)]}{1-\exp[-\lambda_k T + i(\omega_k T - 2\pi j)]/N} + \frac{1}{N}\sum_{r=0}^{N-1} w_r \exp(-i2\pi rj/N). \tag{9a}$$

Equation (9a) shows that there is no obvious direct relation between that values G_j and A_k except for those components for which the frequencies ω_k are integer multiples of the frequency interval $\Delta\omega = 2\pi/T$. *For these particular components* with $j = K$ and $\omega_k = K2\pi/T$, we have

$$G_K = A_K \frac{1-\exp(-\lambda_K T)}{\lambda_K T} + \frac{1}{N}\sum_{k=0, k\neq K}^{N-1} A_k \frac{1-\exp[-\lambda_k T + i(\omega_k T - 2\pi j)]}{1-\exp[-\lambda_k T + i(\omega_k T - 2\pi j)]/N} + \frac{1}{N}\sum_{r=0}^{N-1} w_r \exp(-i2\pi rj/N), \tag{9b}$$

provided that λ_K is small.

It can be seen that if all the values λ_k vanish for k running from 0 to $N-1$, we have

$$G_K = A_K + O\left(\frac{1}{N}\right) + W(K), \tag{9c}$$

where $O(1/N)$ is the contribution of the remaining components and $W(K)$ is the noise contribution.

In the latter case, G_K thus directly yields the value of A_K disregarding the contribution of the noise. The term $O(1/N)$ shows that the contribution of the remaining components is of order $1/N$. More generally, the frequency of a component can be related to two successive integer multiples of $\Delta\omega$ as

$$K\,\Delta\omega \leqslant \omega_K \leqslant (K+1)\,\Delta\omega \tag{10a}$$

or

$$(K-1)\,\Delta\omega \leqslant \omega_K \leqslant K\,\Delta\omega. \tag{10b}$$

In practice, K corresponds to the values of j for which G_j is a peak in the spectrum despite the leakage effect. Equations (10) can be expressed as

$$\omega_K = (K+\varepsilon_K)\,2\pi/T, \qquad \text{with} \quad 1 \geqslant |\varepsilon_K|. \tag{10c}$$

The interpolation method consists in determining ε_k from which ω_k is then obtained by using Eq. (10c). We can isolate the contribution of the peak of order K in Eq. (9a) and Eq. (2) yields

$$G_j = \frac{1}{N} A_K \frac{1-\exp[i2\pi(F_K T - j)]}{1-\exp[i(2\pi/N)(F_K T - k)]} + \frac{1}{N} \sum_{k=0, k\neq K}^{N-1} A_k \frac{1-\exp[i2\pi(F_k T - j)]}{1-\exp[i(2\pi/N)(F_k T - j)]} + W(j), \tag{11a}$$

where we have

$$F_k = \Omega_k/2\pi = i\frac{\lambda_k}{2\pi} + f_k = i\frac{\lambda_k}{2\pi} + (k+\varepsilon_k)\frac{1}{T} \tag{11b}$$

for k running from 0 to $N-1$ and

$$W(j) = \text{the discrete Fourier transform of the noise } w(t_r).$$

For the values K of the integer j, the contribution of the peak of order K is dominant compared with that of the remaining components. We thus have

$$G_K = A_K \frac{1-\exp z_K}{-z_K} + O_K\left(\frac{1}{N}\right) + W(K), \tag{12}$$

where we have

$$z_K = i2\pi(F_K T - K) = -\lambda_K T + i2\pi\varepsilon_K \tag{13}$$

$$O_K\left(\frac{1}{N}\right) = \frac{1}{N} \sum_{k=0, k\neq K}^{N-1} A_k \frac{1-\exp i2\pi(F_k T - K)}{1-\exp i\dfrac{2\pi}{N}(F_k T - K)}. \tag{14}$$

Similarly for $j=K+1$ and $j=K-1$, we have

$$G_{K+1}=A_K\frac{1-\exp z_K}{-z_K+i2\pi}+O_{K+1}\left(\frac{1}{N}\right)+W(K+1) \tag{15}$$

$$G_{K-1}=A_K\frac{1-\exp z_K}{-z_K-i2\pi}+O_{K-1}\left(\frac{1}{N}\right)+W(K-1). \tag{16}$$

The line shape fitting method described in [3] needs the calculation of the differences

$$S^+=G_K-G_{K+1} \tag{17}$$

$$S^-=G_K-G_{K-1}. \tag{18}$$

These quantities involve the difference of terms as $O_K(1/N)-O_{K-1}(1/N)$. It can be easily shown that for sufficiently high value of N we have

$$\begin{aligned} &O_K\left(\frac{1}{N}\right)-O_{K+1}\left(\frac{1}{N}\right)\\ &\quad=i\frac{2\pi}{N^2}\sum_{k=0,k\neq K}^{N-1}A_k\\ &\qquad\times\frac{[1-\exp z_k]\left[\exp i\frac{2\pi}{N}(k-K+\mu_k)\right]}{\left[1-\exp i\frac{2\pi}{N}(k-K+\mu_k)\right]\left[1-\exp i\frac{2\pi}{N}(k-K+\mu_k-1)\right]}, \end{aligned} \tag{19}$$

where $\mu_k=z_k/i2\pi$.

Equation (19) shows that the contribution of the components of order k different from K is of order $1/N^2$ in the computation of S^+. A similar derivation leads to a similar result for the value of the difference S^-. The essence of the procedure consists in determining the parameter ε_k, from which ω_k is then obtained by using Eq. (10b). The value of ε_k is deduced from that of the complex number z_k defined in Eqs. (13) and (20):

$$\frac{S^+}{S^-}=\frac{G_K-G_{K+1}}{G_K-G_{K-1}}=\frac{i2\pi+z_K}{i2\pi-z_K}. \tag{20}$$

Equations (12), (15), (16), (19), and (20) show that the contribution of the components of order k different from K—that are the so-called "remaining components"—is of order $1/N^2$ and we have

$$z_K=i2\pi\frac{G_{K+1}-G_{K-1}}{2G_K-G_{K+1}-G_{K-1}}. \tag{21}$$

It should be noticed that the contribution of the noise has been partly eliminated in the calculation of z_K as was shown in [3], provided that its Fourier transform is gradually varying.

II.3.2. *Use of Hanning Window*

We present in this section the effect of the Hanning window function on the error computation involved in the method [7]. Equations (2), (3.b), (6), (8) yield

$$G_j = \frac{1}{N} A_K \frac{1-\exp i2\pi(F_K T - j)}{1-\exp i(2\pi/N)(F_K T - j)} + O_j\left(\frac{1}{N}\right)$$
$$-\frac{1}{2N} A_K \frac{1-\exp i2\pi(F_K T - j - 1)}{1-\exp i(2\pi/N)(F_K T - j - 1)} - \frac{1}{2} O_{j+1}\left(\frac{1}{N}\right)$$
$$-\frac{1}{2N} A_K \frac{1-\exp i2\pi(F_K T - j + 1)}{1-\exp i(2\pi/N)(F_K T - j + 1)} - \frac{1}{2} O_{j-1}\left(\frac{1}{N}\right) + W(j),$$

where $O_j(1/N)$ is defined in Eq. (14).

For $j = K$, the contribution of the component of order K is predominant as it was for the case of a rectangular window. We thus have

$$G_K = \frac{A_K}{i2\pi} \cdot \frac{1-\exp(i2\pi\mu_K)}{-\mu_K} + O_K\left(\frac{1}{N}\right)$$
$$-\frac{1}{2}\frac{A_K}{i2\pi} \cdot \frac{1-\exp(i2\pi\mu_K)}{-\mu_K+1} - \frac{1}{2} O_{K+1}\left(\frac{1}{N}\right)$$
$$-\frac{1}{2}\frac{A_K}{i2\pi} \cdot \frac{1-\exp(i2\pi\mu_K)}{-\mu_K-1} - \frac{1}{2} O_{K-1}\left(\frac{1}{N}\right) + W(K),$$

where μ_K is defined in Eq. (22),

$$\mu_k = z_k / i2\pi \tag{22}$$

and z_k is defined in Eq. (13).

Further calculations lead to Eq. (23),

$$G_K = A_K \frac{1}{2i\pi} P(\mu_K)[1-\exp(i2\pi\mu_K)] + \sigma(K) + W(K), \tag{23}$$

where we have

$$P(\mu_K) = \frac{1}{\mu_K(\mu_K+1)(\mu_K-1)} \tag{24}$$

and

$$\sigma(K) = O_K\left(\frac{1}{N}\right) - \frac{1}{2} O_{K-1}\left(\frac{1}{N}\right) - \frac{1}{2} O_{K+1}\left(\frac{1}{N}\right). \tag{25}$$

The σ_k values represent the contribution of the remaining components. It should be noticed that in some sense the leakage effect is illustrated by the multiplicative factor before A_K and the additive factor σ_k is a part of the error. It is easy to show that this error is significantly reduced compared with the error defined in the case of the rectangular window if one writes Eq. (25) in the following form:

$$\sigma(K)=\frac{1}{2}\left[O_K\left(\frac{1}{N}\right)-O_{K-1}\left(\frac{1}{N}\right)\right]-\frac{1}{2}\left[O_{K+1}\left(\frac{1}{N}\right)-O_K\left(\frac{1}{N}\right)\right].$$

After some manipulations, Eq. (19) yields successively

$$\sigma(K)=\frac{i2\pi}{2N^2}\sum_{k=0,\,k\neq K}^{N-1}\times\frac{A_K\exp i(4\pi/N)(k+\mu_k-K)(1-\exp z_k)[\exp(-i2\pi/N)-\exp(+i2\pi/N)]}{[1-\exp(i2\pi/N)(k+\mu_k-K-1)]\times[1-\exp(i2\pi/N)(k+\mu_k-K)][1-\exp(i2\pi/N)(k+\mu_k-K+1)]}$$

$$\sigma(K)=\frac{-4\pi^2}{N^3}\sum_{k=0,k\neq K}^{N-1}\times\frac{A_K\exp i(4\pi/N)(k+\mu_k-K)(1-\exp z_k)}{[1-\exp(i2\pi/N)(k+s_k-K-1)]\times[1-\exp(i2\pi/N)(k+\mu_k-K)][1-\exp(i2\pi/N)(k+\mu_k-K+1)]},$$

provided that N is sufficiently large.

The latter expression shows that σ_k is of order $1/N^3$ while its value is of order $1/N$ in the case of a rectangular window. We thus have

$$\sigma(K)=O(1/N^3). \tag{26}$$

It is now possible to compute the values G_j for $j=K+1$ and $j=K-1$. This leads to the equations:

$$G_{K+1}=A_K\frac{1}{2i\pi}P(\mu_K)\frac{\mu_K-1}{\mu_K+2}[1-\exp(i2\pi\mu_K)]+\sigma(K+1)+W(K+1) \tag{27}$$

$$G_{K-1}=A_K\frac{1}{2i\pi}P(\mu_K)\frac{\mu_K+1}{\mu_K-2}[1-\exp(i2\pi\mu_K)]+\sigma(K-1)+W(K-1). \tag{28}$$

As was shown in the case of a rectangular window, the values z_k and μ_k are computed by using the ratio $(G_K-G_{K+1})/(G_K-G_{K-1})$ in order to partly eliminate the noise contribution. We thus have

$$\frac{G_K-G_{K+1}}{G_K-G_{K-1}}=-\frac{\mu_K-2}{\mu_K+2}=-\frac{z_K+i4\pi}{z_K-i4\pi}. \tag{29}$$

We can now determine the complex value z_k. It represents a complex value of the complex frequency shift similar to that was introduced by Feit and Fleck [8]. We have

$$z_K = i4\pi \frac{G_{K+1} - G_{K-1}}{2G_K - G_{K+1} - G_{K-1}}. \tag{30}$$

Equations (23, (24), (26), (30) show that the improvement expected by using a Hanning window function is achieved. The previous development also illustrates the mechanism of reduction of the error by using the contiguous values of the spectrum. This is an answer to a question of Feit and Fleck [8].

III. Computation of the Components' Characteristics

From Eqs. (11b), (21), and (30) the complex frequency can be determined by the formulae

$$z_K = i2\pi\nu \frac{G_{K+1} - G_{K-1}}{2G_K - G_{K+1} - G_{K-1}} \tag{31}$$

$$\lambda_K = \frac{(-1)}{T} \operatorname{Re}\{z_K\} \tag{32}$$

$$\varepsilon_K = \frac{1}{2\pi} \operatorname{Im}\{z_K\} \tag{33}$$

$$F_K = (\varepsilon_K + K)\frac{1}{T} + i\frac{\lambda_K}{2\pi}, \tag{34}$$

where we have

$\nu = 1$ for a rectangular window

$\nu = 2$ for a Hanning window.

The complex amplitudes are derived by using the values of z_k and $2G_K - G_{K+1} - G_{K-1}$. This technique is a local interpolation as described in [3], since the contiguous values of G_K, G_{K+1} and G_{K-1} have been used. It can be shown that this leads to

$$A_K = (2G_K - G_{K+1} - G_{K-1}) \frac{z_K(z_K^2 + 4\pi^2)}{8\pi^2(1 - \exp z_K)} \tag{35}$$

for a rectangular window and to

$$A_K = (2G_K - G_{K+1} - G_{K-1}) \frac{i\pi(4 - \mu_K^2)}{6P(\mu_K)(1 - \exp z_K)} \tag{36}$$

for a Hanning window function, where z_k is defined in Eq. (13) and $P(\mu_k)$ in Eq. (24). The accuracy of these values depends upon the accuracy of z_k and μ_k values and the efficiency in eliminating the noise contribution.

An alternative method for computing the complex amplitudes consists of resolving the linear system related to amplitude values once the frequencies and damping are computed. This technique is a global method [8] and it is used in the time domain methods. This will be described in Section IV.

IV. Applications of the Method

IV.1. *Application of the Method to a Class of Signals Encountered in a Nuclear Magnetic Resonance Field (NMR)*

The spectral interpolation is applied to a theoretical signal defined in Eq. (37). This signal is similar to those encountered in a NMR field. It is a superposition of eight components constituted of two groups of the so-called triplets centered around 1 and 3 KHz and a group of doublets around 9 Khz:

$$g(r\,\Delta t) = \sum_{j=1}^{8} a_k \exp[(-\lambda_k + i2\pi f_k) r\,\Delta t + i\varphi_k)]. \tag{37}$$

The results are reported in Table I. Each component has been computed by using rectangular and Hanning function. On each line of the Table I, the actual value and calculated values are reported. The improvement of the accuracy is observed. The weighted data are more accurate and exhibit one more significant digit than the unweighted data.

The error exhibited in the third line for each component is the lowest one; specifically, the computed amplitude exhibits error of order 10^{-2} and the damping values exhibit errors of order 10^{-5} for weighted data instead of respectively about 10^{-1} and 10^{-4} for the rectangular one. More generally, the frequencies and the damping values are more accurate than the amplitudes and phases values. The reason lies in the essence of the method that involves the use of the frequency shift for the computation of the complex frequency. In other words, the error propagated into the frequency calculation is only due to the error exhibited in the calculation of the frequency shift.

It should be noted that the effective accuracy is much lower than the one predicted by the theory in Eqs. (12), (26), (27). This is essentially due to the proximity effect, that is to say, the proximity of frequencies inside the triplet and the doublet of the signal. Further investigations of the proximity effect are shown in [7]. We only

TABLE I

Comparison between the Actual Values of the Components Characteristics for a Signal Defined in Eq. (37)

k	a_k arbitrary units	f_k (kHz)	λk (kHz)	ϕk (degrees)
1	2.0	0.95	0.0	0.0
Rectangular	1.932124	0.949832	0.000493	2.86
Hanning	2.008280	0.950024	0.000061	−0.41
2	3.0	1.00	0.0	0.0
	2.983196	0.999849	0.00040	2.74
	2.999190	1.000027	−0.000020	−0.49
3	2.0	1.05	0.0	0.0
	1.926941	1.050162	−0.000463	−2.65
	2.007846	1.049980	0.000053	0.34
4	2.0	3.00	0.0	0.0
	1.925751	2.999802	0.000567	3.43
	2.009946	3.000030	0.000076	−0.52
5	4.0	3.05	0.0	0.0
	3.980471	3.049906	−0.000016	3.44
	4.000910	3.050017	−0.000003	−0.29
6	2.0	3.10	0.0	0.0
	1.913719	3.100187	−0.000513	−3.10
	1.985926	3.100062	−0.000158	−1.17
7	8.0	9.00	0.0	−90.0
	7.906643	8.999874	−0.000315	−87.56
	8.024332	9.000026	0.000066	−90.49
8	8.0	9.05	0.0	90.0
	8.145153	9.049903	0.000241	91.66
	7.979368	9.050015	−0.000038	89.73

Note. $N = 2048$; $\Delta t = 0.50$ ms. The signal is not noised. The calculations are performed in double precision on an IBM PC.

present some numerical tests in order to point out the degradation of the accuracy for very close frequencies. The tests were performed on the signal defined in Eq. (38) that consists of two components with frequencies only separated by some percents of kilohertz. The proximity parameter e is defined as this distance between two frequencies. This value is the number of the numerical linewidths $1/T$. The accuracy is then degraded by decreasing the values of the parameter e:

$$g(t) = a_1 \exp(-\lambda_1 t) \cos(2\pi f_1 t + \varphi_1) + a_2 \exp(-\lambda_2 t) \cos\left[2\pi\left(f_1 + e\frac{1}{T}\right)t + \varphi_2\right]. \tag{38}$$

The calculations have been performed on a set $N = 2048$ samples, a time interval $\Delta t = 0.05$ ms. We also have $\phi_1 = \phi_2 = \lambda_1 = \lambda_2 = 0$. The quantity e takes values running from 0 to 13. The results are presented in Fig. 1, where the evolution of the number of significant digits is shown versus the values of the parameter e. It can be seen that the number of significant digits is reduced by half as soon as the proximity parameter value is lower than 12. The method is not able to separate the components for the values of e lower than 3.

Another test is the analysis of the noise effect; this is important to appreciate some measurement of the reliability of the method for real signals. Such a test has been performed on a theoretical signal defined in Eq. (39), where we have superimposed a synthesized white noise:

$$g(t) = a \exp(-\lambda t) \cos(2\pi f t + \varphi) + w(t). \tag{39}$$

The noise $w(t)$ is generated by the classical routines RANDU and GAUSS. The parameters values are $a = 1.0$, $f = 1$ Khz, $\phi = 0$, $\lambda = 0$, $N = 2048$, and $\Delta t = 0.5$ ms. The mean value of $w(t)$ is zero. The results reported in Fig. 2 illustrate the evolution of the significant digits versus the noise variance σ^2. The computations are performed in double precision on an IBM-compatible PC. It can be seen that the loss of accuracy is important since the number of significant digits is halved as soon as the noise variance takes the value 0.01. However, the computed values remain reasonably accurate for the frequency and the damping and, to a lesser extent, for the amplitude and the phase.

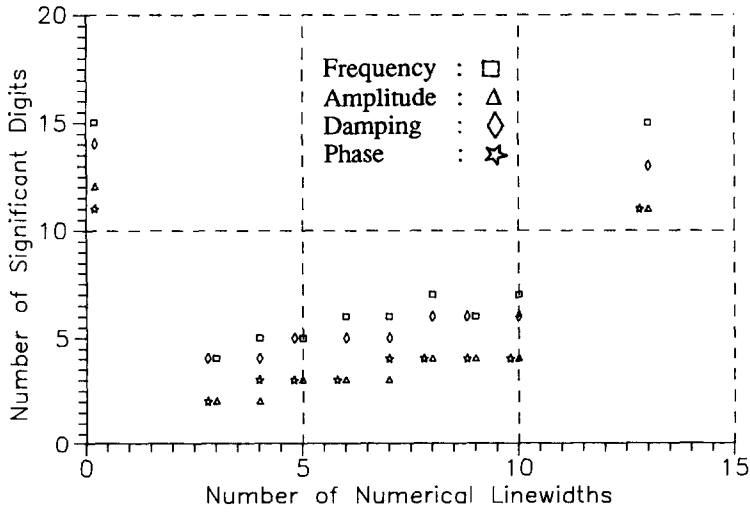

FIG. 1. Numerical experiments showing the proximity effect. The number of significant digits versus the numerical linewidths number e. The signal $g(t)$ is given by Eq. (38); $N = 2048$; $\Phi_1 = \Phi_2 = \lambda_1 = \lambda_2 = 0$; $f_1 = 3$ kHz; $f_2 = f_1 + e/T$; $\Delta t = 0.05$ ms.

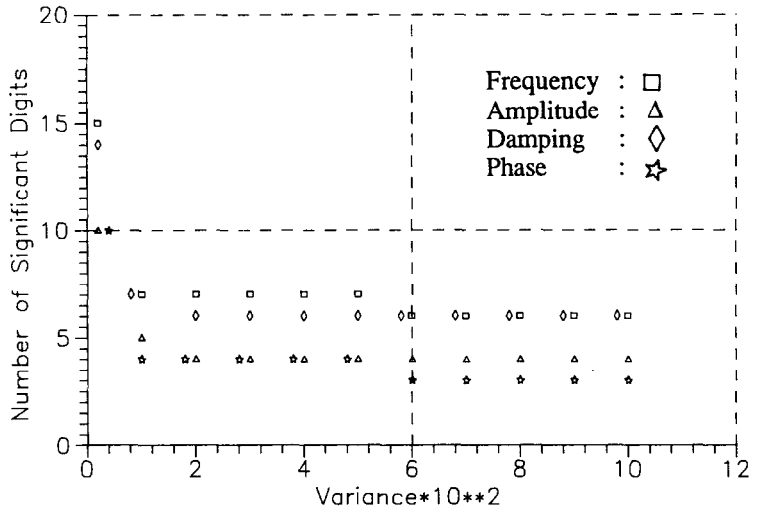

FIG. 2. Numerical experiments showing the noise effect. The number of significant digits versus the noise variance σ^2. The signal $g(t)$ is given by Eq. (39); $N = 2048$; $\Phi = \lambda = 0$; $f = 3$kHz; $w(t) = 0$; $\Delta t = 0.05$ ms.

IV.2. *Comparison of the Present Method with That of Ref.* [10]

This section is devoted to the comparison of the spectral interpolation method with a time domain method. It is well known that the retrieval of the components characteristics of pseudoperiodic signals can be achieved by using a time domain approach that does not need the calculation of the discrete Fourier transform. The selected signal for the analysis is a simulated and a real NMR free induction decay (FID) of ethanol. The main difficulty of the analysis lies in the quartet around 1.0 KHz which is very difficult to depict.

IV.2.1. *Review of the Method of Ref.* [7]

The time domain method—the so-called LPSVD (linear prediction singular value decomposition)—is based on a linear prediction method. It is derived from a Kumaresan and Tufts method [11]. The value of the signal at time t_r is assumed to be a linear combination of the K previous (or future) values. The LPSVD method is an autoregressive (AR) method. An extensive list of time domain methods can be found in the paper by Kay and Marple [9]. We have focused the comparison with the method developed by de Beer and Van Ormondt. It can be shown that a signal consisting of a superposition of K [illegible] Eq. (40), can be expressed in terms of an AR model of order $2K$, Eq. (41):

$$g_r = \sum_{k=1}^{K} C_k \exp(-\lambda_k r\,\Delta t)\cos(2\pi f_k r\,\Delta t + \varphi_k) + w(r\,\Delta t) \tag{40}$$

$$g_r = a_1 g_{r-1} + a_2 g_{r-2} + \cdots + a_M g_{r-M}, \qquad \text{with} \quad r = 1, 2, \ldots, N. \tag{41}$$

M is the AR order and $M = 2K$. The first step of the method is to compute the a_r values by using the matrix expression of Eq. (40). The numerical resolution is a least square method. Specifically, the linear system to be solved is

$$[\mathbf{G}][A] = [g], \tag{42}$$

where

$[\mathbf{G}]$ is a $2K \times (N - 2K)$ matrix

$[A]$ is the column of the $N - 2K$ autoregressive coefficients

$[g]$ is the column of $N - 2K$ samples g_r.

An efficient method based upon the singular value decomposition of the matrix $[\mathbf{G}]$ is then used to compute the autoregressive coefficients.

The second step is the calculation of f_k and λ_k by solving a polynomial of order M. It is shown that the roots of the polynomial of Eq. (43) are conjugate complex and the real and imaginary parts are respectively related to the damping and the frequency. For a large value of M, numerical instabilities can occur during the root calculation in Eq. (43),

$$z^{2K} - a_1 z^{2K-1} - \cdots - a_{2K-1} z - a_{2K} = 0, \tag{43}$$

and this makes the use of the method delicate.

The last step is the computation of the amplitudes C_k and the phases ϕ_k. At this stage a second linear system is solved, since Eq. (40) is equivalent to Eq. (44):

$$\sum_{k=1}^{K} C_k \cos \varphi_k \exp(-\lambda_k r\, \Delta t) \cos(2\pi f_k r\, \Delta t) - \sum_{k=1}^{K} C_k \sin \varphi_k \exp(-\lambda_k r\, \Delta t) \sin(2\pi f_k r\, \Delta t) = g_r. \tag{44}$$

IV.2.2. *Results and Discussions*

The analysis of both simulated and experimental NMR FID of ethanol is illustrated in Tables II and III. In Table II the results obtained by using the LPSVD method [9] are compared with those of the present method in the case of a signal without noise. One can find the actual values on the first line. For a number of samples equal to 1024 there is no error in computing the components characteristics by using LPSVD. The LPSVD algorithm has been implemented by de Beer and Van Ormondt on a SUN-3/160 workstation in single precision while the interpolation spectral method results are obtained from an IBM PC in double precision in order to allow the comparison; $N = 4096$ samples were needed for the analysis. The results obtained by the spectral method are reasonably accurate. The computing times are quite different because about 21 min are needed for the

TABLE II

Parameters of Eight Damped Sinusoids, Fitted to the Simulated NMR FID of Ethanol (without Noise)

k	a_k arbitrary units	f_k (kHz)	λk (kHz)	ϕk (degrees)
1				
LPSVD	41.79	0.4697	−0.0135	0.0
FFT	41.79	0.4697	−0.013500	0.0
2				
LPSVD	50.00	1.0311	−0.0028	0.0
FFT	51.00	1.031091	−0.002757	1.4
3				
LPSVD	150.00	1.0381	−0.0028	0.0
FFT	149.71	1.038101	−0.002804	0.0
4				
LPSVD	150.00	1.0451	−0.0028	0.0
FFT	150.10	1.045102	−0.002798	−0.4
5				
LPSVD	50.00	1.0521	−0.0028	0.0
FFT	49.58	1.052106	−0.002816	−0.8
6				
LPSVD	150.00	2.2662	−0.0028	0.0
FFT	148.56	2.266200	−0.002801	−0.1
7				
LPSVD	300.00	2.2732	−0.0028	0.0
FFT	299.86	2.273201	−0.002801	−0.1
8				
LPSVD	150.00	2.2802	−0.0028	0.0
FFT	149.35	2.280204	−0.002808	−0.7

Note. $N = 1023$ for LPSVD; $N = 4096$ for FFT. The exact values are set to be the values computed by the LPSVD method.

LPSVD method while only 2 min are required for the FFT method. It should be noted that for the case of a signal without noise the components are accurately computed by LPSVD method even if only 300 samples are used.

The results corresponding to the real signal shown in Fig. 3 are reported in Table III. It can be seen that the accuracy in computing frequencies is quite similar. However, the FFT technique exhibits a more stable evolution of the phases and more accurate values of the amplitudes. This means that the use of the LPSVD technique cannot be separated from difficulties related to the noise effect; specifically, the choice of significant frequencies is a determinant, since it should be related to the number of components M. In addition, when the number of samples is large, numerical instabilities can occur in the polynomial roots calculation. A method

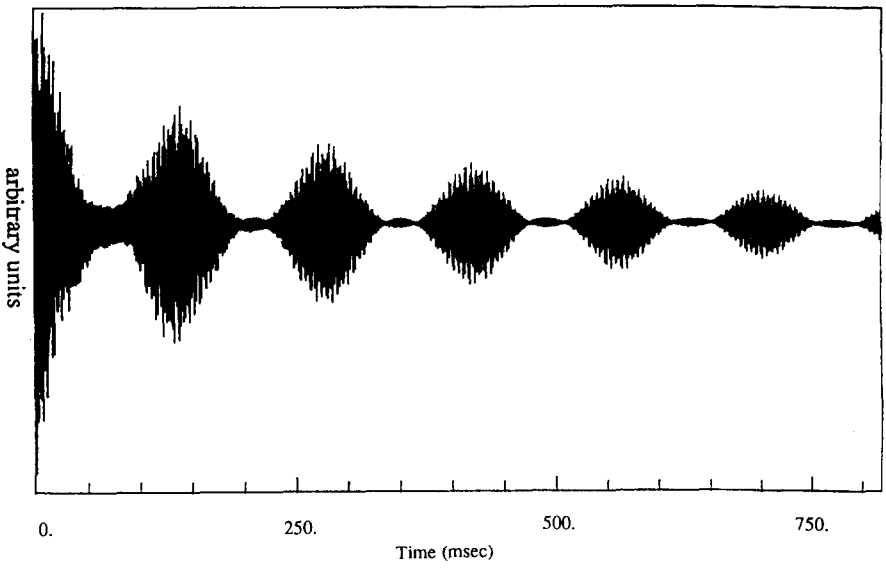

FIG. 3. First 4096 data points of the experimental NMR FID of Ethanol.

involving a direct resolution of the matrix in Eq. (42) is shown in [9] by using Hankel singular value decomposition. Although no polynomial root finding is needed, the computing time remains very long and the method requires a greater memory allocation; at last the lack of stability in phase values is also observed.

The effect of frequency shift is illustrated in Fig. 4. The quartet is analyzed and the values computed by using direct FFT (symbol "Δ") are compared with those obtained by the interpolation method ("|").

IV.3. *Application of the Method to a Class of Numerical Signals Encountered in an Optical Field*

It should be instructive to examine some results obtained by applying the method to a class of signals encountered in an optical field. Those signals usually describe a complex potential [8]. The analysis is shown on the case of a theoretical complex signal defined in Eq. (45)

$$g(t) = \sum_{k=1}^{10} \exp(-i\beta_k t), \tag{45}$$

where $\beta_k = \beta_k^r + i\beta_k^i$.

Such a signal is similar to a correlation function and is useful for studying the mode properties of optical fibers with lossy components [8]. It should be noticed that the present method does not require a specific algorithm for the analysis of a complex signal. This constitutes a significant advantage compared with the algorithms used in the time domain methods for which specific algorithms are required respectively for real and complex signals.

TABLE III

Parameters of the Eight Largest Damped Sinusoids, Fitted to the Experimental NMR FID of Ethanol Measured by Haasnoot *et al.*, University of Nymegen [9]

k	a_k arbitrary units	f_k (kHz)	λk (kHz)	ϕk (degrees)
1				
LPSVD	333	0.4699	−0.0149	−68.9
FFT	339.1	0.4696	−0.0107	−63.3
2				
LPSVD	81	1.030	−0.008	11.0
FFT	54	1.0310836	−0.00204	−60.5
3				
LPSVD	90	1.0379	−0.0030	−129
FFT	150.0	1.037925	−0.002181	−55
4				
LPSVD	264	1.0470	−0.004	−129
FFT	148	1.0450	−0.002081	−51
5				
LPSVD	365	1.0498	−0.015	−28
FFT	47	1.0520	−0.001458	−49
6				
LPSVD	209	2.2658	−0.00	−128
FFT	141	2.2658	−0.00197	−39
7				
LPSVD	315	2.2728	−0.00	70
FFT	267	2.2729	−0.0024	−33
8				
LPSVD	173	2.2803	−0.00	84
FFT	128	2.2800	−0.0016	−27

Note. $N = 1024$ for the time domain method; $N = 4096$ for the spectral method.

The results are shown in Table IV. A comparison with the results published by Feit and Fleck is made. It can be seen that the single-line fit used in the present spectral interpolation leads to results in good agreement with those of Feit *et al.* These authors have used a multiple line least square fit for their test.

In order to show how sensitive the present method is, another numerical test has been performed on a signal defined in Eq. 46, where the fourth component has a very low amplitude value compared with the nine others (0.005 against 1.0),

$$g(t) = \sum_{k=1;k\neq 4}^{10} A_k \exp\{(-i\beta_k^r + \beta_k^i)_t\} + A_4 \exp\left\{\left(-i\left(\beta_5^r + e\frac{2\pi}{T}\right) + \beta_4^i\right)t\right\}, \qquad (46)$$

where $A_4 = 0.005$ and $A_j = 1.0$ for j running from 1 to 10 and $j \neq 4$.

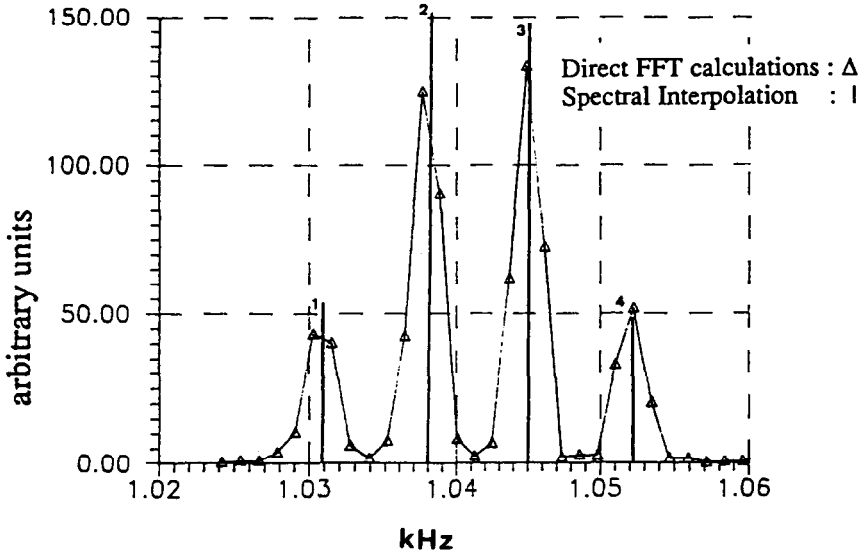

FIG. 4. Spectral analysis of the quartet of the experimental NMR FID of Ethanol. The data-points are weighted by a Hanning function. The symbols "△" are the direct FFT results Gj (Eq. (2)). The vertical lines are related to the spectral interpolation (Eqs. (31) to (36)).

TABLE IV

Comparison between the Actual Values of the Complex Frequencies for a Spectrum with Ten Peaks and the Values Predicted by the Method Used in [8] and in the Present Study

Actual values			Computed values multiple line least square (Ref. [8])			Computed values single line fit (present method)			
A_n	β_n^r	β_n^i	A_n	β_n^r	$\beta_n^i \times 10^{10}$	A_n	$\text{Arg}(A_n) \times 10^6$	β_n^r	$\beta_n^i \times 10^9$
1.0	800.0	0.0	1.000000	800.0000	2.14	1.000000	0.59	800.0000	−7.97
1.0	760.0	0.0	1.000000	760.0000	2.01	1.000000	0.79	760.0000	4.69
1.0	720.0	0.0	1.000000	720.0000	1.97	1.000000	−1.14	720.0000	4.83
1.0	680.0	0.0	1.000000	680.0000	2.09	1.000000	−2.77	680.0000	2.71
1.0	640.0	0.0	1.000000	640.0000	2.33	1.000000	3.26	640.0000	1.14
1.0	600.0	0.0	1.000000	600.0000	2.34	1.000000	2.00	600.0000	4.09
1.0	560.0	0.0	1.000000	560.0000	2.22	1.000000	0.12	560.0000	5.25
1.0	520.0	0.0	1.000000	520.0000	2.08	1.000000	−1.80	520.0000	4.32
1.0	480.0	0.0	1.000000	480.0000	1.98	1.000000	−3.14	480.0000	1.41
1.0	440.0	0.0	1.000000	440.0000	1.95	1.000000	1.91	440.0000	3.92

Note. The amplitudes A_n are complex in the present method. $N = 8200$; $\Delta t = 0.00375$ cm.

The proximity effect is accounted by introducing the parameter e in Eq. (46) as was done in Section IV.2. The results are shown in Table V for $e = 180$ and for the values of the other parameters identical to those presented in Table IV. It can be seen that the accuracy of the computed values are very good. However, the β_4^i value related to the fourth component is computed with an error of 1.17×10^{-8} instead of values around 10^{-10} for the remaining components. A similar observation can be made for the argument value of the complex amplitude A_4. This lack of accuracy is due to the low value of the fourth component amplitude. This means that the sensitivity of the method can be analyzed by decreasing the values of the proximity parameter e and by counting the number of significant digits for the characteristics components.

Such a test has been performed and the results are illustrated in Figs. 5 to 8. For

is similar to that of the fifth one. The proximity parameter values e run from 3 to 180; for each value of e, the number of significant digits related to the real spatial frequency β_n^r and the absolute value of A_n are shown on Figs. 5 and 7. The computed values of the damping β_n^i and the argument of A_n are illustrated in Figs. 6 and 8. For each value of e the results corresponding to the fifth component ($A_5 = 1.0$) are shown by the symbol "△" and those related to the fourth component ($A_4 = 0.005$) by the symbol "□."

It can be seen that the accuracy is significantly lowered for the fourth component. Specifically, for large values of e (e higher than 40), the number of significant digits of the real part of β is halved and we have 7 instead of 13; however, it remains reasonable. For moderate values of e the number of significant digits is still

TABLE V

Analysis of a Signal Having a Very Low Amplitude Component

	Actual values				Computed values			
n	A_n	$\mathrm{Arg}(A_n)$	β_n^r	β_n^i	A_n	$\mathrm{Arg}(A_n) \times 10^8$	β_n^r	$\beta_n^i \times 10^{10}$
1	1.0	0.0	800.0000	0.0	1.000000	−1.84	800.0000	0.95
2	1.0	0.0	760.0000	0.0	1.000000	−0.33	760.0000	2.93
3	1.0	0.0	720.0000	0.0	1.000000	1.07	720.0000	0.98
4	0.005	0.0	676.8155	0.0	5.000000×10^{-3}	−3.02	676.8155	117.0
5	1.0	0.0	640.0000	0.0	1.000000	−3.65	640.0000	1.80
6	1.0	0.0	600.0000	0.0	1.000000	2.17	600.0000	0.57
7	1.0	0.0	560.0000	0.0	1.000000	−0.05	560.0000	3.44
8	1.0	0.0	520.0000	0.0	1.000000	−2.27	520.0000	1.08
9	1.0	0.0	480.0000	0.0	1.000000	−0.14	480.0000	2.99
10	1.0	0.0	440.0000	0.0	1.000000	1.36	440.0000	0.93

Note. The signal is defined in Eq. (46); $e = 180$, $N = 8200$, $\Delta t = 0.00375$ s.

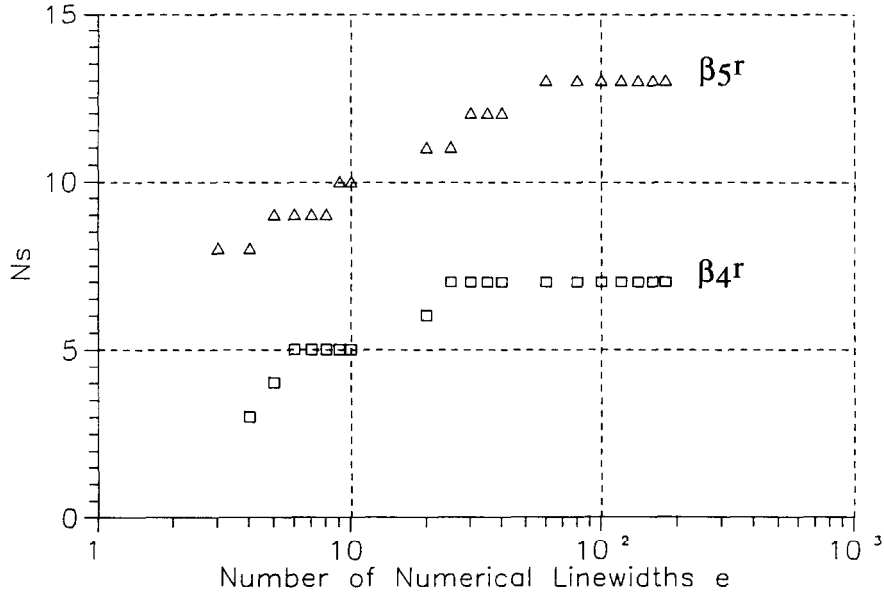

FIG. 5. Analysis of the sensitivity of the spectral interpolation method for the number of significant digits of β_4^r and β_5^r values. The complex signal is defined in Eq. (46); $N = 8192$; $\Delta t = 0.00375$ cm.

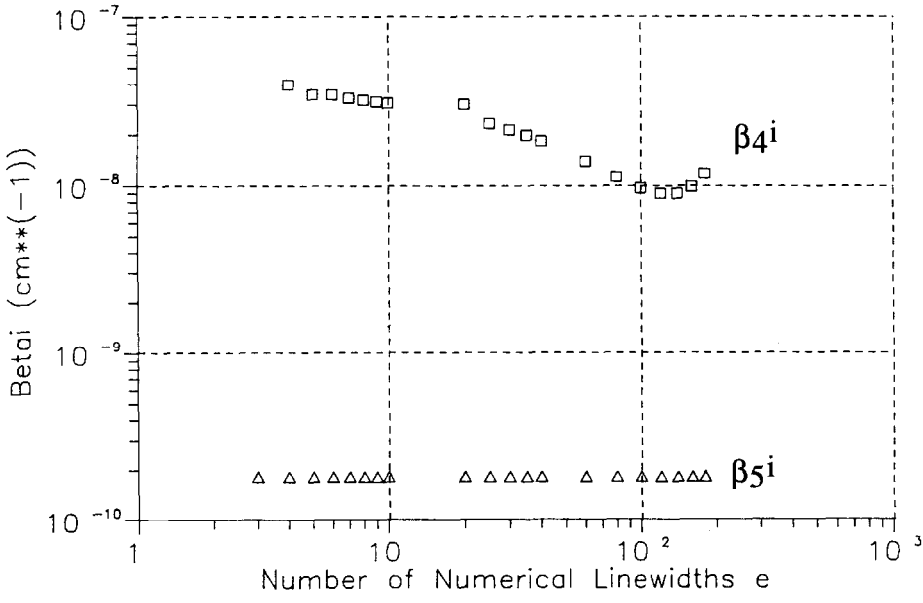

FIG. 6. Analysis of the sensitivity of the spectral interpolation method for the computed values of β_4^i and β_5^i; the actual values are $\beta_4^i = \beta_5^i = 0$. The complex signal is defined in Eq. (46); $N = 8192$; $\Delta t = 0.00375$ cm.

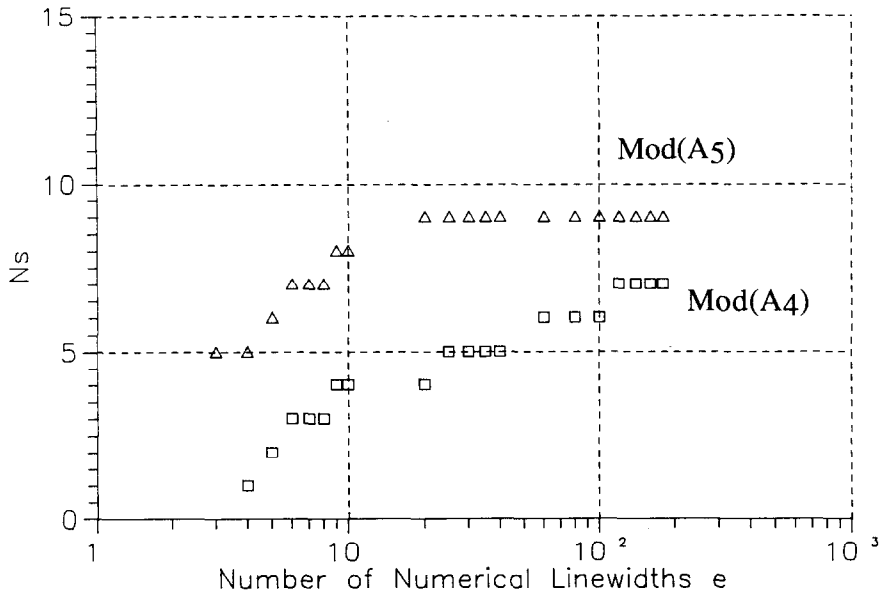

FIG. 7. Analysis of the sensitivity of the spectral interpolation method for the number of significant digits of Mod(A_4) and Mod(A_5) values. The complex signal is defined in Eq. (46); $N = 8192$; $\Delta t = 0.00375$ cm.

reasonable (higher than 11 for β'_5 and equal to 7 for β'_4). For low values of e ($e < 10$), the accuracy is clearly degraded and the number of significant digits falls down respectively to 8 for β'_5 and to 3 for β'_4 (Fig. 5).

Figure 6 illustrates the evolution of the computed values of the imaginary part of β versus the number of the numerical linewidths e. It can be seen that the values corresponding to the fifth component are very accurate (10^{-10} instead of 0.0); in addition, these values are not modified by the proximity of the fourth component. The imaginary part values β'_4 are less accurate.

The number of significant digits of the module $|A_n|$ for $n = 4$, 5 and the computed values of Arg(A_n) are respectively shown in Figs. 7 and 8. These values are less accurate than those related to the complex frequencies as was already observed in the case of real signals. Once again the number of significant digits is roughly halved for the fourth component characteristic values compared with those of the fifth component values (Fig. 7). At last the most illustrative graphs to show the accuracy degradation are in Figs. 8a and b. The arguments Arg(A_4) take values up to 123° instead of 0.0° for very low values of e (Fig. 8a). It can be seen that the error growth is quasi-exponential (Fig. 8a). In the case of two very close frequencies for which we have a small amplitude line near a high amplitude line, a multiple line least square fit should be preferred in lieu of a single line fit as was observed by Feit *et al.*

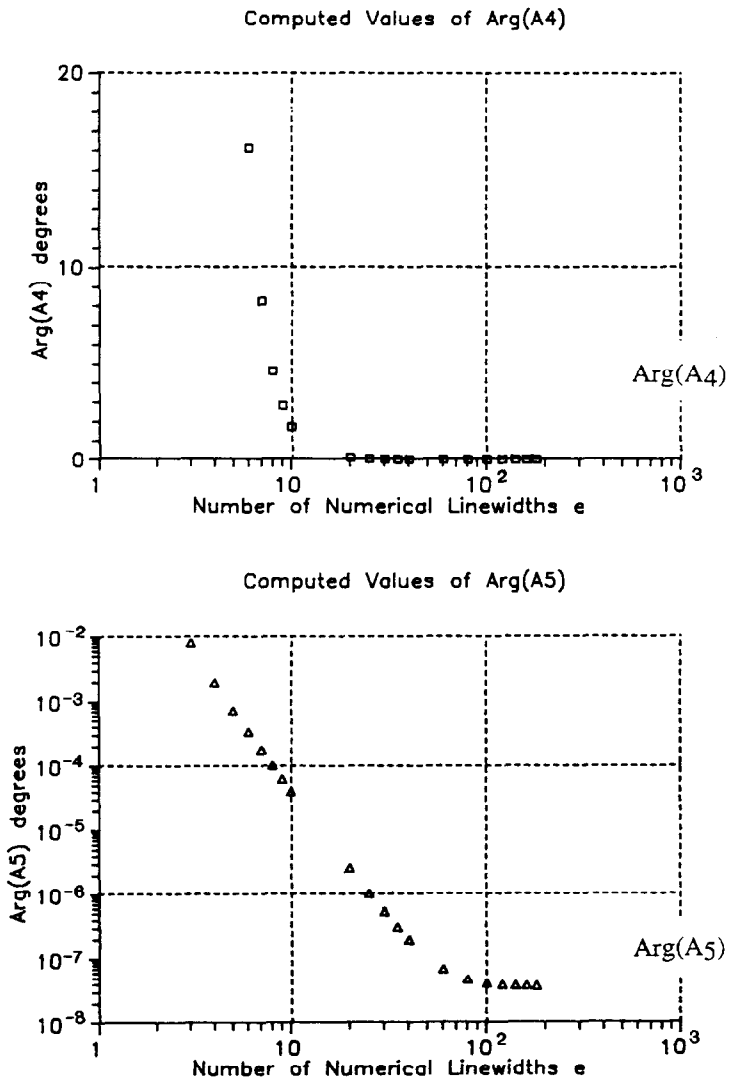

FIG. 8. Analysis of the sensitivity of the spectral interpolation method for the computed values of $\mathrm{Arg}(A_4)$ and $\mathrm{Arg}(A_5)$; the actual values are $\mathrm{Arg}(A_4) = \mathrm{Arg}(A_5) = 0$. The complex signal is defined in Eq. (46); $N = 8192$; $\Delta t = 0.00375$ cm.

These numerical tests show that two spectral lines four numerical linewidths apart can be distinguished; however, the accuracy can be dramatically lowered. In practice the method is reliable for values of the parameter e higher than 10. The computations corresponding to Tables IV, V, and Figs. 5 to 8 have been performed on a Vax 8700 in double precision. The number of samples was $N = 8192$; the spatial step was 0.00375 cm.

V. Conclusions

The accuracy of the spectral method described in [3] has been studied. The error has been expressed in terms of the contribution of the remaining components. The mechanism of reducing the error has been clearly demonstrated by using the peak of the spectrum for which three consecutive values are used. In addition, it has been shown that the analysis of data weighted by a Hanning window function naturally involves the foregoing procedure and leads to higher accuracy. The efficiency of the method has been compared with a time domain method. The following concluding remarks can be given:

— The spectral interpolation is a reliable method for computing the components of a pseudoperiodic signal. The frequency and damping calculations are more accurate compared with the complex amplitude calculations. This is due to the fact that the complex amplitudes are computed by using the complex frequency shift that is likewise computed with some errors.

— A parameter responsible for degrading the accuracy is the proximity parameter that is in some sense a measurement of the distance between two frequencies. The spectral interpolation is able to separate the quartet frequencies of an NMR FID of ethanol for a duration of observation of 750 ms, including 4096 samples.

— The sensitivity of the method is related to its capability to depict a low amplitude spectral line in the vicinity of a high-amplitude spectral line. Numerical tests have shown that, in general, about 10 numerical linewidths are required to give a reasonable accuracy.

— A comparison of the spectral interpolation with a time domain method shows that the width of the window function must be sufficiently large in order to increase the frequency separation capability. Once the frequencies are separated the spectral method is very numerically efficient. On the other hand, the time domain method is able to compute the characteristics of the components even for a low number of the samples. Unfortunately, the computation of very close frequencies requires a large number of samples. As a consequence, numerical instabilities and prohibitive time computation cannot be avoided. At last, in the case of the real ethanol signal, a loss of stability in the phase calculation is observed. This means that the LPSVD method is very sensitive to the noise effect and to the sample number.

— At last, the method has been also applied to the analysis of both theoretical and experimental hydrodynamic phenomena [7, 2]. These investigations have been devoted essentially to the study of vortex shedding in the flow past a circular cylinder at subcritical Reynolds numbers.

ACKNOWLEDGMENTS

The authors are indebted to Dr. de Beer and Dr. Van Ormondt for discussions and the exchange of numerical codes. They are also acknowledged for having transmitted the experimental results performed by Haasnot *et al.* in the University of Nymegen. We also greatly thank Dr. Feit for his support and encouraging remarks. The reviewers are greatly acknowledged for their advice and suggestions.

REFERENCES

1. M. D. FEIT, J. A. FLECK, JR., AND A. STEIGER, *J. Comput. Phys.* **47**, 412 (1982).
2. Y. LECOINTE AND J. PIQUET, in *Proceedings 16th Symposium on Naval Hydrodynamics, Berkeley*, 1986.
3. R. D. RAJAONA AND P. SULMONT, *J. Comput. Phys.* **61**, 186 (1985).
4. S. A. ORSZAG, *Stud. Appl. Math.* **51**, 3 (1972).
5. O. E. BRIGHAM, *The Fast Fourier Transform* (Prentice–Hall, Englewood Cliffs, NJ, 1974).
6. F. J. HARRIS, *Proc. IEEE* **66**, 5 (1978).
7. R. D. RAJAONA, Thèse de Doctorat d'Etat, University of Nantes, 1987 (unpublished).
8. M. D. FEIT AND J. A. FLECK, JR., *Appl. Opt.* **20**, 5 (1981).
9. R. DE BEER, Department of Applied Physics, Technical University of Delft (unpublished).
10. H. BARKHUIJSEN, R. DE BEER, M. J. BOVEE, AND D. VAN ORMONDT, *J. Magn. Reson.* **61**, 465 (1985).
11. R. KUMARESAN AND D. W. TUFTS, *IEEE Trans. Acoust. Speech Signal Process.* **ASSP-30**, 833 (1982).
12. S. M. KAY AND S. L. MARPLE, in *Proc. IEEE* **69**, No. 11, 1380 (1985).